Understanding the Surface Condition of Silicone Rubber Nanocomposite due to Corona Ageing Using AFM Imaging and LIBS Spectroscopy

Baskar Thangabalan, Neelmani, Neelesh J Vasa, Ramanujam Sarathi, Noureddine Harid, and Huw Griffiths

***Abstract*—Silicone rubber insulators undergo degradation when they are exposed to corona discharges. The present study explores the surface degradation behavior of silicone rubber alumina nanocomposites due to corona ageing using high-frequency AC voltage. The electric field distribution on the sample surface during corona ageing is simulated using COMSOL. The change in silicone rubber functional group is studied using Fourier transform infrared spectroscopy (FTIR) analysis. The influence of corona ageing time on the surface roughness recovery of silicone rubber nano alumina composites is studied using an atomic force microscope (AFM). The elemental distribution behavior and change in the emission spectra persistence time are analyzed during recovery period of corona-aged silicone rubber nanocomposites using Laser-Induced Breakdown Spectroscopy (LIBS) technique. The addition of alumina nanofiller to the silicone rubber improves the resistance to ageing due to corona discharge. Loss and recovery of hydrophobic property of silicone rubber due to corona aging were determined using static contact angle measurement. The results show a direct correlation between the contact angle and the surface roughness recovery characteristics. They indicate that the nanocomposite having a 5 wt% alumina content exhibits the highest resistance to corona discharge with least surface damage. Furthermore, fast recovery was observed in the first few hours after corona ageing, and most samples eventually regained their properties after about 8 hours of recovery time.**

Index Terms— Silicone rubber, Nanocomposites, Corona discharges, Surface roughness, Hydrophobicity, Recovery

I. INTRODUCTION

SILICONE rubber insulators are increasingly gaining acceptance for use in transmission and distribution systems because of their better dielectric performance, hydrophobic nature, vandal resistance, lightweight to strength ratio, good pollution performance, and good performance in harsh environments [1-4]. Recent research has shown that alumina added silicone rubber nanocomposites show improved erosion resistance and enhanced thermal stability [5, 6]. The optimum addition of nano-silica to the silicone rubber showed better performance under accelerated multi-stress weathering conditions. The low molecular weight (LMWs) loss and polymer functional groups scission process from the surface is greatly reduced due to the strong bonding of silanol groups with nanofiller. Venkatesulu et al. demonstrated the benefit of nano alumina and micro-ATH filled silicone rubber composite in improving the resistance to electric discharge and concluded that the performance of the nanocomposite is better than that of the micro composite due to the enhanced thermal stability and better physical bonding of the nanofiller with the polymer chain [7].

One of the major problems in outdoor insulators is the surface degradation of the insulating material caused by corona discharges. The corona discharge can produce ozone, intense UV radiation, and ion deposition on the surface of the insulator causing functional group variations. Many researchers investigated the ageing of silicone rubber by corona and concluded that the addition of a small number of nanoparticles to the polymer base matrix increases the barrier resistance of the polymer chain and improves the surface erosion and degradation resistance to multiple ageing parameters including corona discharge. Considerable works were carried out to understand the impact of the corona discharge to silicone rubber [8-10]. Maoqiang Bi et al., have indicated that corona ageing of silicone rubber in high humid zone can cause intense damage to the material [11]. Banerjee et al., studied the performance of silicone rubber nanocomposites aged in different pressure condicitons and they have concludedthat increase in pressure results in increased corona discharges and loss of hydrophobicity of the material [12].

It is known that the hydrophobicity transfer is mainly due to the migration of low molecular weight (LMW) polymer chains from the bulk to the surface of the silicone rubber to restore the low surface energy [13-15]. This corona-induced change in surface roughness impacts the hydrophobicity recovery characteristics of silicone rubber depending on the corona ageing period and nanofiller loading.

One of the useful techniques that have been used for characterizing the surface morphology of aged samples is Atomic Force Microscope (AFM) technique. Gao et al. studied the surface morphology during the loss and recovery of the hydrophobicity of aged HTV silicone rubber using AFM and wavelet transform analysis [16]. LIBS is one of the useful

Baskar Thangabalan is with Department of Electrical Engineering, Indian Institute of Technology Madras, Chennai, India.

Neelmani is with Department of Electrical Engineering, Indian Institute of Technology Madras, Chennai, India.

Neelesh J Vasa is with Department of Engineering Design, Indian Institute of Technology Madras, Chennai, India.

Ramanujam Sarathi is with Department of Electrical Engineering, Indian Institute of Technology Madras, Chennai, India (e-mail:rsarathi@iitm.ac.in).

Harid Noureddine with the HVDM research group, Khalifa University, Abu Dhabi, United Arab Emirates.

Huw Griffiths is with Cardiff University, Cardiff CF24 3AA, UK

noninvasive tools to analyze the qualitative and quantitative changes in the elemental compositions of the materials [17]. Wang et al. studied the LIBS spectra of the silicone rubber nanocomposites and observed the change in the spectral characteristics due to the change in the physical and chemical properties after ageing [18]. Furthermore, the impact of corona discharge on the surface characteristics of the material, including hydrophobicity and tracking/erosion, are reported using diagnostic procedures including image saturation, digital image processing, and nuclear resonance magnetic detection [19,20]. Neelmani et al. investigated the impact of corona discharges on the surface morphology characteristics of the nanocomposites by measuring contact angle, and surface profile measurement using atomic force microscopy (AFM) and characterized the AFM spectra obtained by adopting the multiresolution signal decomposition (MRSD) technique [21]. However, the impact of filler loading and, change in surface morphology due to LMW migration during the corona ageing recovery period, and the elemental distribution behavior of the sample due to corona discharge is scanty

This paper reports the results of a study on silicone rubber nanocomposites subjected to corona ageing to elucidate the following important aspects using AFM and LIBS techniques (i) analysis of surface roughness at different ageing periods, (ii) recovery characteristics of silicone rubber nanocomposite at a different time intervals, (iii) analysis of the hydrophobicity loss and recovery behavior by use of contact angle measurement, (iv) analysis of elemental distribution and plasma emission persistence time of silicone rubber alumina nanocomposites under corona discharge using LIBS during the recovery time.

II. Experimental Studies

A. Sample Preparation

The alumina nanofiller (99.9%, 100 nm average size of particles, Hongwu Nanometer, China) is dried in the oven for 24 hours at 150º C to remove the traces of moisture content. To ensure the proper dispersion of alumina nanofiller the dried nanopowder is mixed with ethanol and kept for ultra-sonication for 30 minutes at 20 kHz. Then the required amount of the silicone rubber base material Part-A' (RTV8112, Momentive, USA) and the alumina-ethanol solution added together, and shear mixed for 30 minutes, then the mixture is kept in the oven at 100º C to evaporate the ethanol. After that, the part B (Hardener RTV9858) is added to the combination in the ratio of 1:10 and trapped air bubbles are removed from the mixture by degasification for 10 minutes. Finally, the alumina- silicone rubber mixture was cast into the mould (100 mm x 100 mm x 1 mm) and kept in compression at a uniform pressure of 10 kg/cm^2 for 12 hours at room temperature helps to maintain the thickness and uniform surface profile of the prepared samples. Similarly, 0, 1, 3, 5, and 10 wt% of alumina-filled silicone nanocomposites are fabricated.

B. Corona Discharge Setup

The corona discharge is produced with the help of a stainless-steel rod-plane electrode setup ,30 kV high-frequency (1.7 kHz) sinusoidal AC voltage as shown in Fig. 1. Corona generated using higher frequency to cause more surface deterioration compared to low frequency or power frequency. The Samples with a size of 2 cm × 2 cm and having a thickness of 3 mm are placed under the electrode, the gap between the electrode tip and the sample is maintained at 5 mm. To observe the electric field distribution on the silicone rubber test specimen, the rod-plane electrode configuration is simulated in COMSOL. The electric field at the centre of the sample is about 6.7 MV/m.

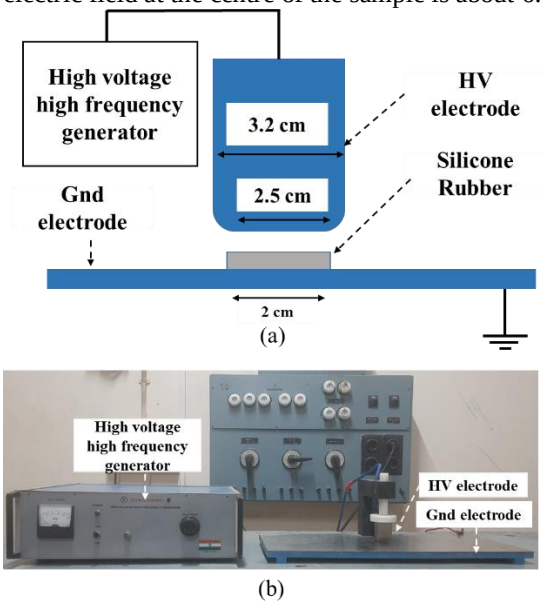

Fig. 1. (a) Typical corona discharge and (b) experimental setup.

C. Roughness Analysis Setup

Surface degradation due to corona ageing increases the sample roughness, hence the surface roughness value is considered as the vital parameter for the assessment of surface degradation. In this study, the 3d surface morphology of sample surface is measured using an atomic force microscope (A 100 AFM: A.P.E Research Srl) equipped with a flexure scanner in non-contact scanning mode. The measurement is carried out with a scan area of 10 μm × 10 μm and the average roughness is calculated. After a different period of corona discharge, the roughness is measured at different time intervals to analyze the surface recovery characteristics.

D. Hydrophobicity Studies

The surface properties of silicone rubber nanocomposite are closely related to the hydrophobic property of its surface. The static contact angle value is used to determine quantitatively the hydrophobicity of the sample, which gives information about the level of surface degradation that occurred due to the corona discharge. The contact angle is measured at different time intervals to analyze the hydrophobicity recovery characteristics. The static contact angle of the sample is measured by placing a 20 μl deionized water on the surface of the sample, and the contact angle (θ) was measured as (1) [22],

This article has been accepted for publication in IEEE Transactions on Dielectrics and Electrical Insulation. This is the author's version which has not been fully edited and content may change prior to final publication. Citation information: DOI 10.1109/TDEI.2022.3214478

$$\theta = 2 * \tan^{-1}\frac{2h}{d} \quad (1)$$

where d and h are the diameter and height of the liquid drop on the sample surface. The measurements were taken at five different locations and averaged.

E. LIBS Studies

A typical LIBS system based on a Q-switched ND-YAG laser (LAB-150-10-S2K, Quanta-Ray LAB series) is shown in Fig. 2. The setup consists of an optical lens, a probe, a transmission fiber, and a spectrometer (USB 2000 by Ocean optics). The pulsed laser energy is adjusted at 30 mJ using Q- switch time delay (1064 nm wavelength, 10 ns pulse width, and pulse repetition rate of 10). The laser energy focused on the sample using the focal lenses, which generates high-temperature plasma. The spectrometer (Ocean Optics USB2000+UV-VIS-ES) and an optical fiber (core diameter 400µm, 0.22 NA) are used to capture the optical emission due to the plasma formation. The intensity and the spectra of the elements present in the sample of the spectral emission are recorded [25]. The spectral elements in the spectra at different wavelengths are identified by using the NIST (National Institute of Standards and Technology) atomic spectra database. Further photodiode connected to the digital storage oscilloscope (DSO) was used to evaluate the plasma emission persistence time for each unaged and corona aged sample. The optical emission was shined on the photodiode using optical fiber and further decay characteristics were measured using DSO.

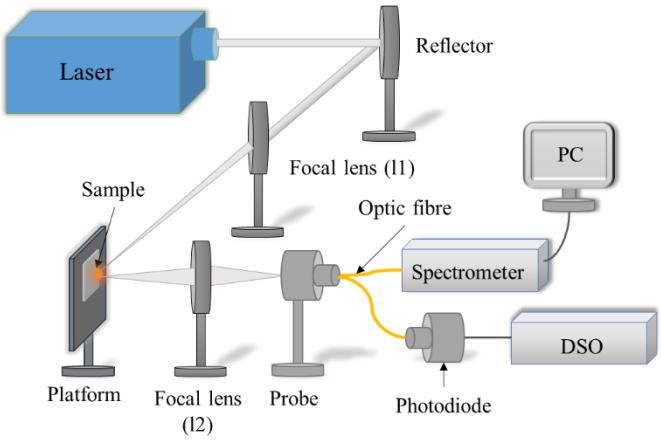

Fig. 2. Typical LIBS setup.

III. Results and Discussion

A. Electric Field Distribution

The corona discharge arrangement shown in Fig. 1 is the exact dimensions were modelled using COMSOL MULTIPHYSICS software. Since the corona discharge arrangement is vertically half symmetry so only the right half side of the setup is modelled as shown in Fig. 3a. In this study, a voltage of 30 kV, 1.7 KHz AC is applied to the top HV terminal and the bottom electrode is grounded. The outer edges of the air background region are given a boundary that assumes there are no outside current and electromagnetic sources. Table I shows the simulation parameters of the corona discharge model.

The simulation was carried out in AC/DC mode using an electric current solver that allows the user to select both conductivity and permittivity of the material. In the AC/DC module, the electric currents are dealt as a time-dependent problem. The advantage of using the time domain is that dielectric displacement field currents can be taken into consideration. The governing equations of the used simulation model are:

$$\nabla . J = Q_j \quad (1)$$

$$J = \sigma E + \frac{\partial D}{\partial t} + J_e \quad (2)$$

$$E = -\nabla V \quad (3)$$

where J is the current density, E is the electric field, D is the electric displacement field and Q_j is the free charge.

TABLE I
SIMULATION PARAMETERS

Relative permittivity of silicone rubber (ε_r)	3.8
Relative permittivity of electrode (ε_r)	1
Conductivity of silicone rubber (S/m)	1.3×10^{-14}
Conductivity of electrodes (S/m)	6.2×10^{6}

The model is simulated for one cycle of the applied voltage (sine wave) and the electric field distribution is observed at different phase angles. The maximum electric field is observed at the 90º phase angle. For all the phase angles the sharp edge of the silicone rubber sample showed a peak electric field whereas uniform electric field distribution is observed in the middle of the sample surface. At the centre of the sample, the electric field of 6.7 MV/m is observed, which is sufficient to generate visible corona between the high voltage electrode and the sample surface. All the analyses in the study were carried out only in this zone. As seen from Fig. 3b, the electric field of 9.5 MV/m, is observed at the sample edge. Admittedly, the dimension of a larger dimension should have been taken for the study, to have the lower electric field at the edges of the specimen.

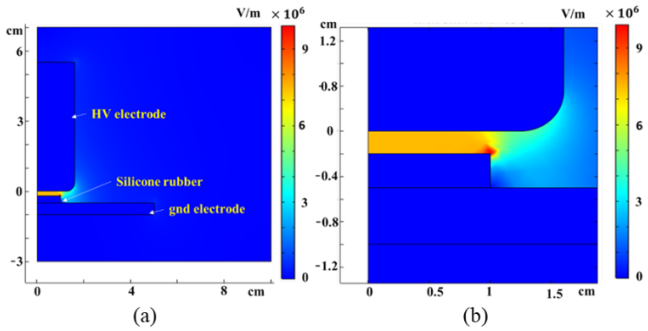

Fig. 3. Electric field distribution during corona discharge (a) typical electric field distribution of rod- plane electrode configuration, at phase angle of 0º (b) electric field distribution at the phase angle of 90º.

B. FTIR analysis

FTIR analysis is used to examine the variation in surface functional groups for corona aged samples. The changes in

This article has been accepted for publication in IEEE Transactions on Dielectrics and Electrical Insulation. This is the author's version which has not been fully edited and content may change prior to final publication. Citation information: DOI 10.1109/TDEI.2022.3214478

these functional groups significantly affect the hydrophobicity, surface morphology and the performance of the silicone rubber under electrical field stress. Figure 4 shows FTIR spectra for 5 wt.% alumina filled unaged and corona aged samples. It is observed that the samples have the same major functional group vibrations. However, many distinct changes in the intensity of the peaks from the FTIR spectra signify changes in the samples after corona ageing of the samples. The different peaks are assigned to the vibration of specific functional groups [26]. C-H bonds in CH_3 groups can be seen at 2960 cm, whereas Si-CH_3 bonds (side chains) can be seen at 1250-1270 cm^{-1} and Si-O-Si bonds (silicone backbones) can be seen at 980-1100 cm^{-1} in the unaged sample. The hydrophilic -OH groups appear in the corona aged silicone rubber spectrum between 3200 and 3600 cm^{-1}.

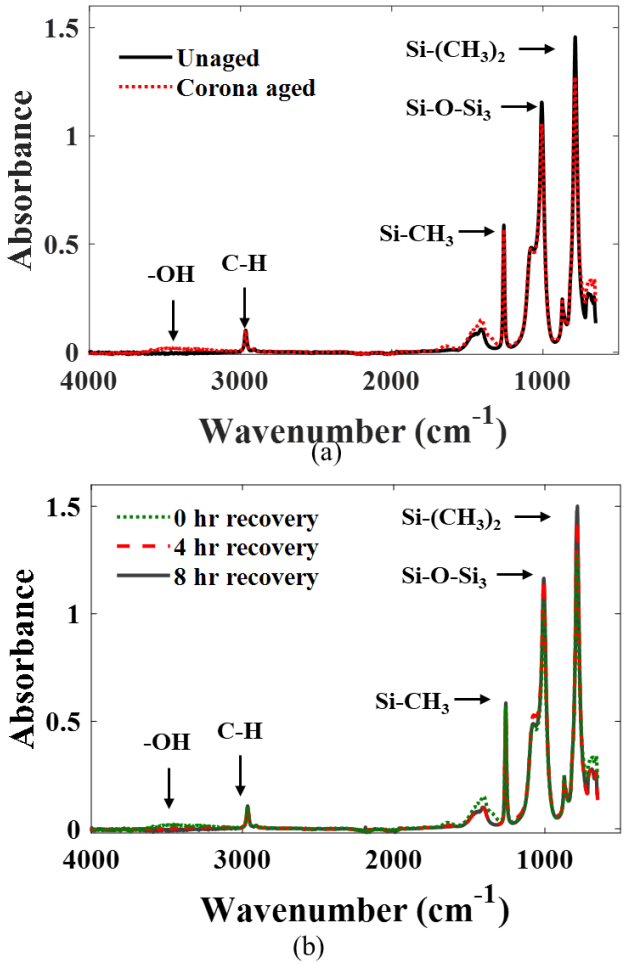

Fig. 4. FTIR analysis of (a) 5 wt.% unaged and 1 hour corona aged silicone rubber alumina nanocomposite, and (b) during recovery period.

After the corona ageing, the C–H, Si–CH_3, and Si–O-Si bonds in the sample dropped significantly compared to the unaged sample. This is because the energy of corona discharge photons is higher than the binding energy of Si-O-Si (8.3 eV) and Si-CH_3 (4.5 eV). Photons released during the corona discharge chop off silicone rubber side chains and backbones [15]. Thus, the corona discharge cuts these methyl groups that are responsible for the hydrophobicity of the material also this chain scission alters the surface morphology. In the presence of oxygen, the corona discharge increased the autoxidation reactions on the surface of the sample. As a result, the O–H bonds, which are hydrophilic groups, were generated as side chains on the surface of the corona-aged sample, replacing the hydrophobic CH_3 groups. This results in a further acceleration of the hydrophobicity loss. After the specimens were exposed to the corona, they were placed in a lab environment and the FTIR analysis was done at specific times. The functional groups of silicone rubber are restored in 8 hours, as depicted in Fig. 4b, due to LMW migration from the bulk of the sample. The absorbance of C–H, Si–CH_3, and Si–O-Si functional groups increases as the recovery period increases, which results in the restoration of hydrophobicity and morphological structure. A similar trend is observed for all wt% of alumina-added silicone rubber nanocomposite samples.

C. Surface Roughness and Morphology of Silicone Rubber Nanocomposite

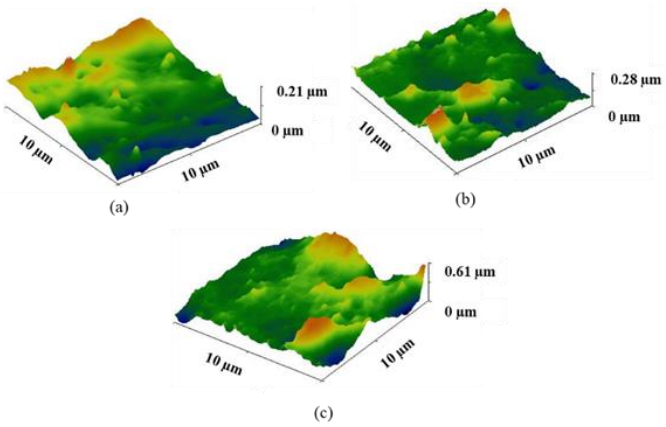

Fig. 5. Typical AFM images of unaged (a) 0, (b) 5, and (c) 10 wt% nano alumina added silicone rubber nanocomposites.

The distribution of alumina nanofiller in silicone rubber is analysed using SEM analysis and shown in our previous study [8]. The adopted method for preparation of nanocomposite sample showed a good dispersion up to 5 wt%, and above that limit, nanoparticles tend to agglomerate. The AFM analysis is carried out on unaged samples and the typical surface profile and the surface roughness magnitude is shown in Fig. 5 and Fig 6. A typical 3D surface profile of unaged 0, 3 and 5 wt% samples measured using AFM, is shown in Fig. 5. It is observed that with the addition of alumina nanoparticles to the silicone rubber the average roughness of the samples is varied. Surface roughness is measured using AFM at three different locations, and the average value was taken. The deviation of the measured average roughness is less than ±10% for all the samples. Among all the samples the pristine silicone rubber possesses a small surface roughness value, and the surface roughness increases with the increase in filler content. At 10 wt% concentration, a much larger (~250%) increase in surface roughness is observed. This reason may be due to the agglomeration of nanofiller in silicone rubber nanocomposites due to strong interactions between the nanoparticles. This leads to the decrease in the interfacial strength between nanofiller and base matrix and causes a change in surface properties like enhanced surface roughness. The roughness of the unaged sample lies in the range

This article has been accepted for publication in IEEE Transactions on Dielectrics and Electrical Insulation. This is the author's version which has not been fully edited and content may change prior to final publication. Citation information: DOI 10.1109/TDEI.2022.3214478

of 86, 92, 97, 102 and 250 nm for 0, 1, 3, 5 and 10 wt% sample respectively.

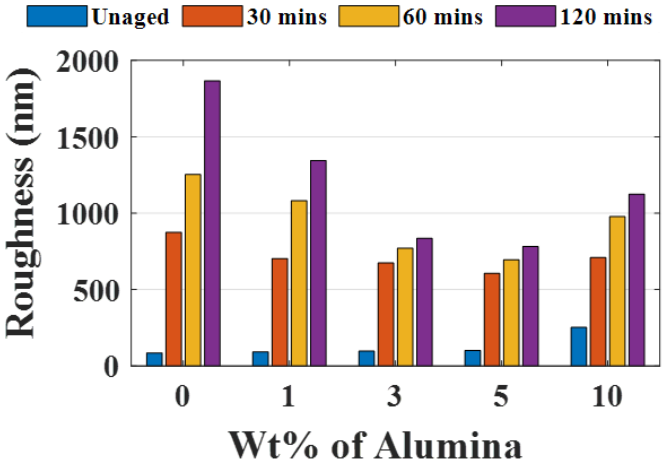

Fig. 6. The roughness of silicone rubber nanocomposites before and after intense corona ageing.

The impact of the corona ageing on the average surface roughness and morphology characteristics of the nanocomposite samples were analyzed using AFM and Fig. 6 shows that the surface roughness after ageing increases with aging duration. A substantial rise in surface roughness is observed and is highest for the virgin sample, reduces to a minimum when the filler concentration increases up to 5 wt%, but starts to increase again at 10 wt% concentration. The roughness increases with the ageing duration, but the higher the concentration of nanofillers is, the smaller is the roughness increment. Similar results were observed by Nazir et al. who concluded that the surface deterioration of pure silicone rubber results in larger cracks, voids, holes, and surface splitting compared to nanocomposites [9]. Intense corona ageing can cause surface cracking of the material, formation of hydroxyl groups due to severe surface oxidation and can increase the surface roughness of the material. Corona discharges cause a change in functional groups of silicone rubber surface, such as deformation of methyl groups into hydroxyl groups and reduction in Si $(CH_3)_2$, Si-O-Si, Si-CH_3, and CH_3(C-H) bond intensity [23]. Furthermore, the C-H bond in CH_3 group Si–C bonds and Si–O bonds are cut off by the corona discharge and combined with OH and OOH groups due to oxidation. These crosslinking and branching of functional groups alter the surface energy and surface morphology of the samples, resulting in sample hydrophobicity loss and a rise in roughness.

In general, the results show that the addition of nanofiller gives improved performance for corona-aged silicone rubber nanocomposites due to the improved resistance to corona ageing [22]. The addition of alumina nanofiller to the silicone base matrix prominently increases the resistance to de-polymerization of $Si(CH_3)_2$ and Si-O-Si as alumina nanofiller introduces an interface between the polymer matrix and the nanoparticles with a strong hydrogen bonding [13]. Hence, the resultant structure acquires a high packing density and is highly resistant to degradation compared to the pure SiR sample. As a result, compared to other samples the increase in corona ageing duration has only a small impact on the 5 wt% sample. At higher wt% of nanofiller, the nanoparticles become agglomerated, resulting in the formation of a weak hydrogen bond, making the surface more prone to degradation.

The reduction in surface roughness increment with ageing duration at 3 wt% and 5 wt % concentrations may be attributed to an increase in interface area and strong chemical bond between the nanofiller and the base matrix, which holds the polymer chain tightly and enhances the resistance of the samples to surface ageing and cracking phenomena. Compared with the unaged samples, 30 min of corona ageing leads to drastic variation in the surface structure of silicone rubber nanocomposites. The pure silicone sample has the largest change in the surface morphology compared to its unaged morphology. It is observed that the 5 wt% sample offers optimum surface morphology change, as an increase in nanofiller concentration worsens the materials' morphology.

D. Recovery Characteristics

After ageing, the samples were allowed to recover in the open air and the recovery characteristics of the surface roughness were monitored for 24 hours at different time intervals. Fig. 7 shows the roughness recovery characteristics after corona ageing. As can be seen from these results, all samples recover substantially within the first 4 hours. The rate of recovery for pure silicone rubber is highest compared to silicone rubber nanocomposite samples. The nanocomposites recovery is based on the reorientation of polar groups, the reduction of a silanol group, and the migration of low molecular weight (LMW) components from the silicone rubber's bulk to the surface [13].

The LMW components have low surface energy and consist of a repeated silicon-oxygen (Si-O) chain and two methyl groups attached with the silicon atom. These methyl groups are mostly responsible for the hydrophobic nature of silicone rubber [16]. Thus, the migration of LMW components reorients the methyl groups which were initially removed from the side of the polymer chain during corona ageing and restores the surface roughness and the contact angle of the silicone rubber alumina nanocomposite. In the case of pure silicone rubber, due to the availability of additional free volume space, migration of LMW components from the bulk to the surface is simple, resulting in a quick recovery of surface roughness. The nanoparticles are compactly arranged in the bulk of the sample due to the strong filler polymer interaction, which hinders the surface degradation process and the movement of LMW components in the polymer chain by restricting any movements in the polymer chain [9]. Consequently, the increase in nanofiller content, surface degradation, and the rate of recovery is reduced. However, at optimum content (5 wt%) of nanofiller, the surface degradation is very low, and the slow recovery rate is no longer a concern. At a higher filler weight content (10 wt%) both the surface roughness and the recovery are increased with the corona ageing period. This is caused by the poor dispersion of the alumina nanofiller which leads to more free volume space in the base matrix and reduces filler polymer bond strength, which eases movement of LMW component in the sample.

This article has been accepted for publication in IEEE Transactions on Dielectrics and Electrical Insulation. This is the author's version which has not been fully edited and content may change prior to final publication. Citation information: DOI 10.1109/TDEI.2022.3214478

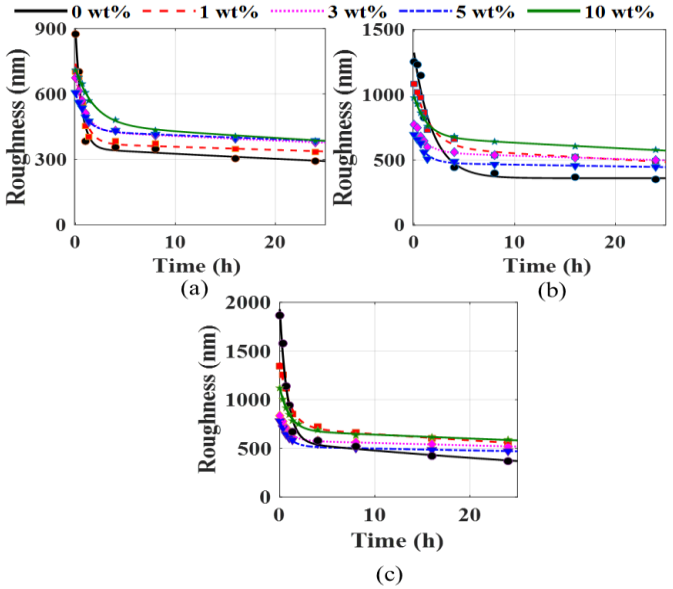

Fig. 7. Surface roughness recovery of silicone rubber nanocomposite after (a) 30 minutes, (b) 60 minutes, and (c) 120 minutes of intense corona ageing.

TABLE II
SURFACE ROUGHNESS RECOVERY RATE OF CORONA AGED SILICONE RUBBER NANOCOMPOSITE

Sample	Surface roughness recovery rate (nm/hr)		
Wt%	30 minutes	60 minutes	120 minutes
0	1.5648	1.651	1.765
1	1.169	1.164	1.167
3	1.041	1.093	1.134
5	0.9838	0.985	1.008
10	0.5358	0.771	0.978

The surface morphology of 60-minute corona aged silicone rubber nanocomposites is demonstrated at various recovery times as shown in Fig. 8. It can be seen that, after 60 minutes of corona exposure, the sample roughness is high and during the recovery period the surface became smoother. It is observed that the smoothness of the pure silicone sample is restored at a faster rate and higher amplitude, whereas slow recovery is observed for nanofiller added samples. Similar characteristics were observed with different wt% of nanofiller added samples. The surface roughness recovery rate of silicone rubber nanocomposite after different corona ageing periods is shown in Table II. With an increase in wt% of alumina nanofiller a reduction in recovery rate is observed. Increases in corona discharge cause increment in the oxygen content and decrement in carbon content in the polymer functional groups, which results in deformation of C-H and Si-CH bonds as it is replaced with oxygen [22]. Hence, with the increase in the corona ageing period, the damage of the polymer chain, and the formation of cracks and voids on the surface increases, this leads to the reduction in resistance to the migration of LMW components and enhances the roughness recovery rate. Additionally, highly mobile LMW components generated as a by-product during corona ageing conceal the surface ageing and contributes to the fast recovery of the sample surface roughness and its hydrophobicity [15]. Hence the recovery rate is higher for pure silicone rubber under severe corona ageing however, it has increased surface roughness and cracks formation. This is a demerit for outdoor insulators because it increases the possibility of pollution accumulation and moisture absorption. A similar increase in surface recovery rate is observed for all silicone rubber nanocomposites at 2 hours of corona exposure.

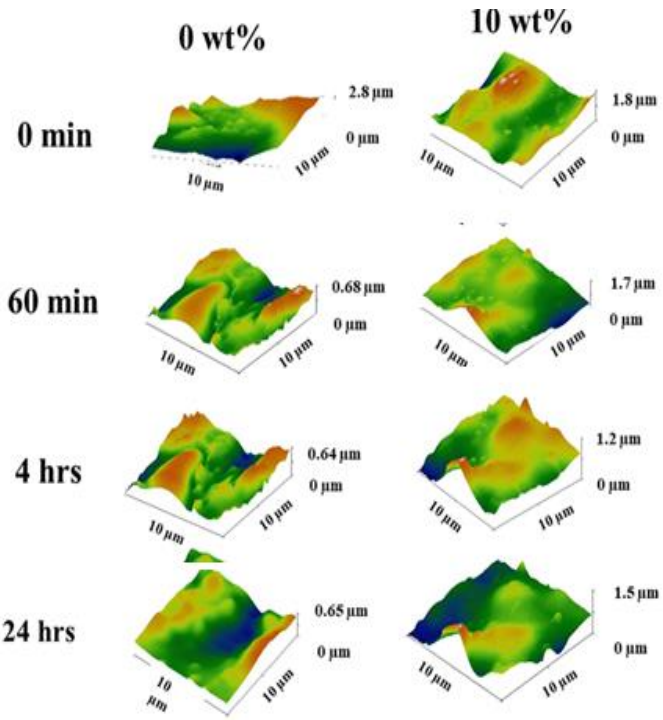

Fig. 8. Surface morphology of roughness recovery of silicone rubber nanocomposite after 60 minutes of intense corona ageing.

E. Hydrophobicity Loss and Recovery Characteristics of Silicone Rubber Nanocomposite

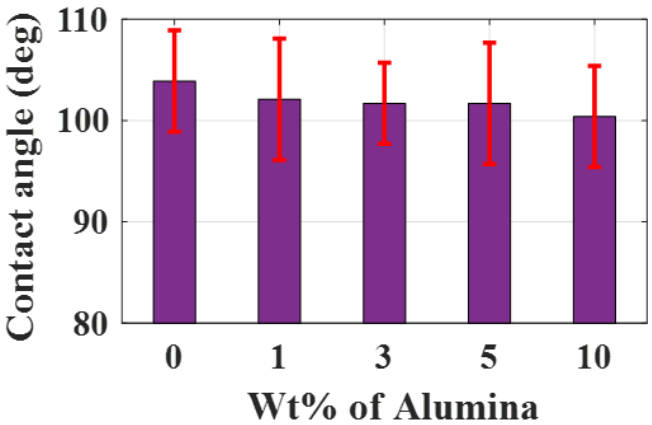

Fig. 9. The static contact angle of unaged silicone rubber nanocomposites.

The hydrophobicity recovery characteristics of aged and unaged samples are assessed by measuring the static contact angle at different recovery periods. The static contact angle of unaged silicone rubber nanocomposite is shown in Fig. 9 and it is observed that the contact angle for all the samples is higher

This article has been accepted for publication in IEEE Transactions on Dielectrics and Electrical Insulation. This is the author's version which has not been fully edited and content may change prior to final publication. Citation information: DOI 10.1109/TDEI.2022.3214478

than 90º confirming the hydrophobic property of the nanocomposites. The addition of alumina nanofiller minimizes the surface energy by reorienting the methyl groups present on the surface of the sample, which results in a small variation in contact angle with the increment in the wt% of alumina nanofiller.

The water droplets present on the silicone rubber insulator surface tend to oscillate under the presence of electric field, this oscillation will alter the electric field distribution and cause localized surface flashover [27]. Fig. 10 shows the pictures of water droplet on sample surface, after 60 minutes corona ageing. The results indicate a drastic reduction in hydrophobicity for all nanocomposites as a result of corona exposure. In all cases, the contact angle was reduced to less than 30º this indicates the dispersion of water droplet on the sample surface. This dispersed water droplet oscillates less under the electric field compared to unaged sample; however, the dispersed water gets easily stretched toward the electrodes under electric field resulting reduced water droplet-initiated corona inception voltage (localized surface flashover) [24]. Thus, the increase in surface roughness due to corona ageing results in more dispersion of water droplet under the applied electric field. Corona discharge causes the loss of methyl groups at the top layer of the silicone rubber which causes the temporary loss of contact angle [9]. Crosslinking between -OH and other functional groups occurs due to corona ageing that forms a hydrophilic group instead of hydrophobic CH_3 groups. As the corona ageing increases the reduction in CH_3 groups from the polymer chain increases that leading to loss of hydrophobicity of the sample.

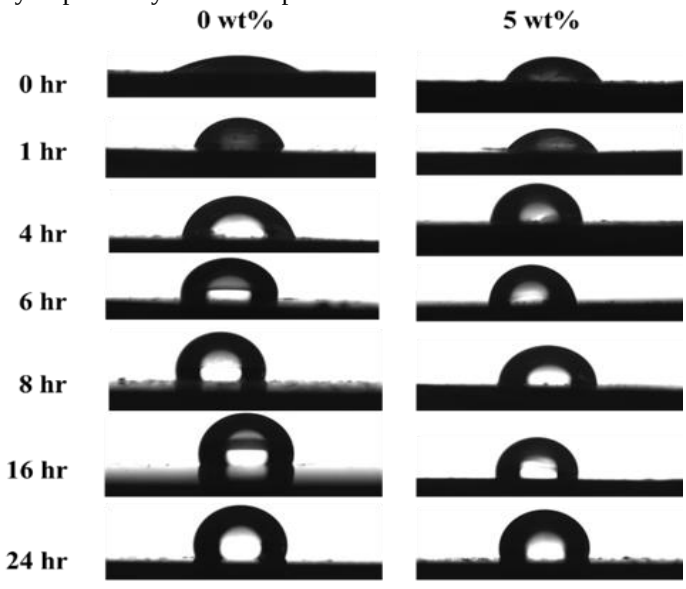

Fig. 10. Images of water droplets showing the hydrophobicity recovery of silicone rubber nanocomposite after 60 minutes of intense corona ageing.

Reduction in the contact angle for the pure silicone rubber sample is highest regardless of the corona ageing period and 5 wt% samples were observed to have less reduction in their hydrophobicity. Corona discharges lead to the accumulation of charges over the surface of samples and produce ions species and ozone. These ionic species and accumulated charges lead to chemical changes on the sample surface. These changes include the increment in oxygen concentration and formation of the hydrophilic hydroxyl (–OH) and silanol (Si-OH) groups on the surface of the sample resulting in the reduction of hydrophobicity [24]. After corona ageing for the different periods, hydrophobicity recovery characteristics were measured in the form of contact angle at different time intervals over 24 hours, as shown in Fig. 11. After corona exposure, the migration of low molecular weight (LMW) components from bulk to surface, reorientation of polar groups, and condensation of silanol are all main factors in the recovery of silicone rubber hydrophobicity [13].

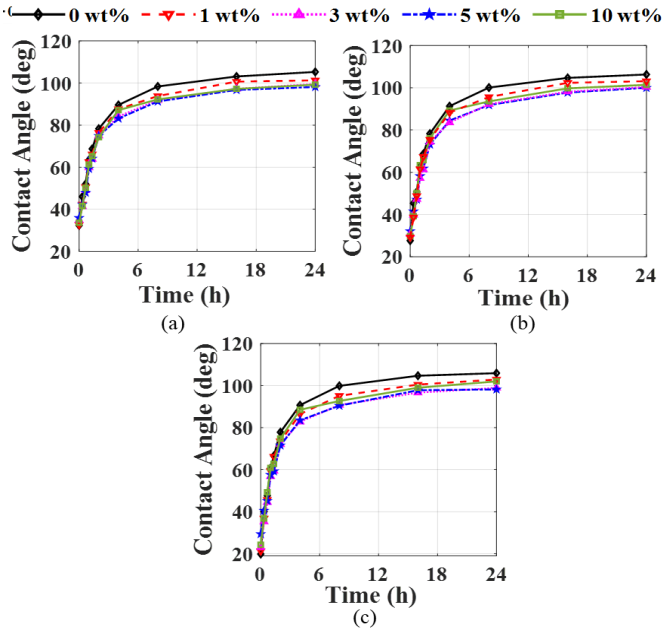

Fig. 11. Hydrophobicity recovery of silicone rubber nanocomposite after (a) 30 minutes, (b) 60 minutes, and (c) 120 minutes of intense corona ageing.

From the experimental results, it is observed that pure silicone rubber has a higher contact angle recovery rate than the different wt% filled silicone rubber nanocomposites and this is due to the relatively easier movement of the LMW components from the bulk to the surface of the sample. In the case of silicone rubber nanocomposites, the strong interaction between the alumina nanofiller and the silicone base matrix offers high resistance to the surface degradation during corona discharge by holding on to the polymer chain. Also, the addition of nanofiller reduces the free volume space available for the movement of LMW components in the polymer chain, which causes the slow recovery of the nanocomposites. A higher level of corona aging results in higher oxidation of the surface, formation of the hydrophilic layer, and formation of surface cracks. The higher contact angle recovery is observed with an increase in the corona ageing period. The creation of surface fissures, which provide a less resistive path for LMW components, may be the source of this increased contact angle recovery. Higher wt% of alumina nanofiller causes agglomeration of the nanoparticles which leads to the weak

This article has been accepted for publication in IEEE Transactions on Dielectrics and Electrical Insulation. This is the author's version which has not been fully edited and content may change prior to final publication. Citation information: DOI 10.1109/TDEI.2022.3214478

bonding with the base silicone rubber matrix and provides more free volume space for the LMW migration. Hence the 10 wt% sample has the worst surface degradation and highest contact angle recovery compared to other nanocomposites.

F. Correlation between Hydrophobicity and Surface Roughness Recovery Characteristics of Silicone Rubber Nanocomposite

Fig. 9 shows that that the contact angle and surface roughness of silicone rubber nanocomposites shows an inverse correlation. It is observed that the surface roughness increases for all samples with an increase in corona ageing time. The increment in the slope with an increase in corona ageing represents the fast recovery characteristics of the sample, also an increase in the initial value with ageing signifies the increment in surface degradation. It is observed that pure silicone rubber has the highest initial value and slope due to its enhanced surface degradation and fast recovery characteristics. The surface roughness and contact angle recovery speed are reduced with an increase in alumina nanofiller wt% as shown in Fig. 7 and Fig. 11. With the addition of 5 wt% filler, the slope remains almost constant for all corona ageing periods. At 10 wt% an increase in slope was observed with the increase in the ageing period, due to the high surface degradation and fast recovery characteristics as mentioned in Fig. 7 A similar trend is observed for all the silicone rubber nanocomposites.

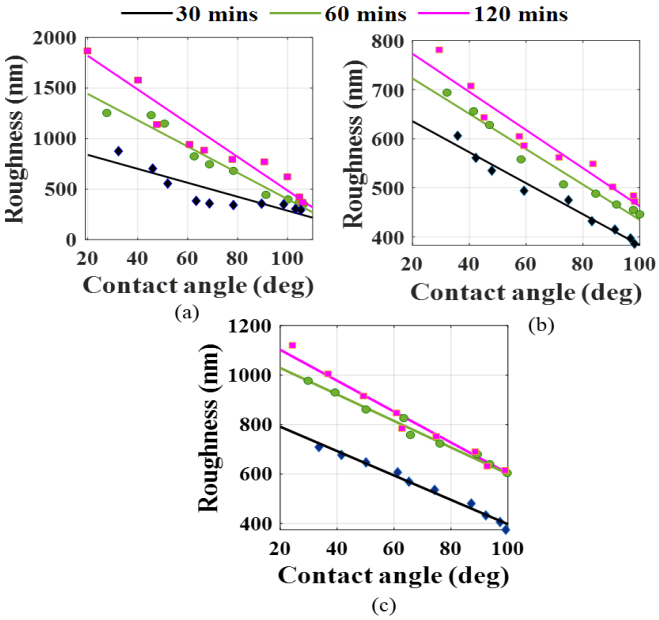

Fig. 12. Correlation between hydrophobicity recovery and roughness recovery (a) 0 wt%, (b) 5 wt%, and (c) 10 wt% of silicone rubber nanocomposites.

G. LIBS Analysis and Elemental Distribution

Fig. 13 shows the typical LIBS spectra of silicone rubber nanocomposites. Dominant peaks of the N(I), N(II), O(I), O(II), Si(I), Si(II), C(I), and C(II) elements were observed in both unaged and corona aged silicone rubber nanocomposites. Neelmani et al. carried out the elemental mapping of the unaged and corona aged samples and calculated the plasma temperature using the Boltzman-Saha equation [21]. From the analysis, they concluded that the plasma temperature of the samples reduced with corona ageing, and within 8 hours of recovery time, the plasma temperature recovers to its initial value.

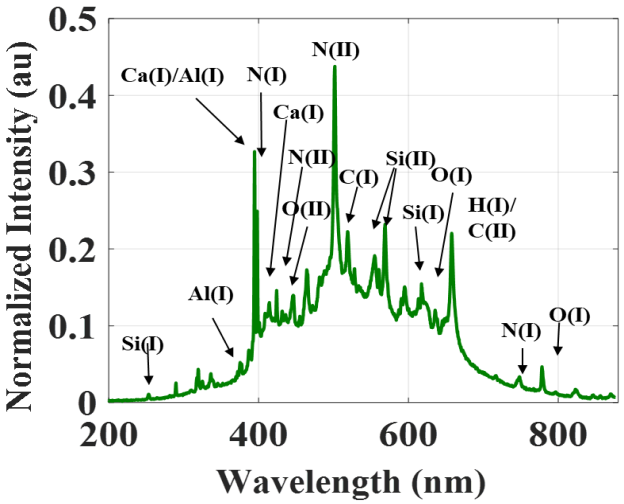

Fig. 13. Typical LIBS emission spectra.

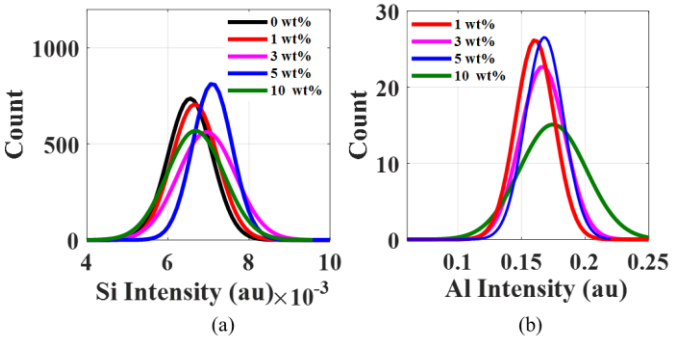

Fig. 14. Distribution diagram of normalized spectral intensity of unaged samples (a) Si, and (b) Al peak.

TABLE III
FULL WIDTH HALF MAXIMUM (FWHM) OF UNAGED AND CORONA AGED SILICONE RUBBER NANOCOMPOSITE

Full Width Half Maximum (FWHM)				
Sample Wt%	Unaged		120 min aged	
	Si (10^{-3})	Al	Si (10^{-3})	Al
0	1.38	-	1.432	-
1	1.328	0.0471	1.421	1.446
3	1.412	0.0433	1.423	1.445
5	1.245	0.0421	1.362	1.402
10	1.482	0.0597	1.492	1.532

In the present work, normalized spectral intensities of Si (λ= 251.6) and Al (λ=396.15nm) peaks are used to characterize the ageing behavior of the nanocomposites. The intensity information of Si and Al lines of all the unaged and corona aged samples are collected at 300 points on the sample surface. Normal distribution analysis is carried out for the intensity of Si and Al peaks of unaged samples as shown in Fig. 14. It is observed that with the increase in the content of alumina nanofiller, the normal distribution curve is distributed around

higher values of peak intensities indicating an increase in the Si peak intensity of the sample. From Fig. 14b similar elemental distribution behavior is observed for Al peaks in nanofiller samples. This is due to the interaction of laser energy with the surface of the sample. As a result, different phenomena like ionization, tunnelling, and avalanche ionization occur, which excite the atoms of the sample surface and cause the ablation. In the case of the nanocomposite samples, more energy will be required to ionize the excited electrons to cause ablation. Hence, during the termination of the laser pulses, the excited electrons of the atoms fall back to their original state by emitting more photons from the plasma, resulting in the increment in the spectral peak intensities [24]. Thus, the observed intensity distribution of the elemental peaks shifted to the higher value of intensity with the addition of nanofiller. Above the optimum filler level, the spectra intensity is reducing due to the poor filler polymer interaction caused by the agglomeration.

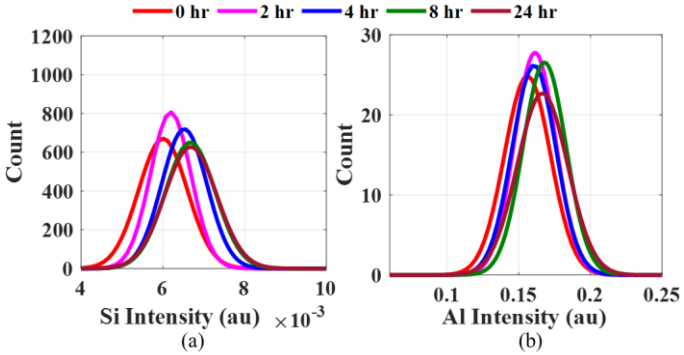

Fig. 15. Normal distribution of 5wt% Si and Al normalized spectral intensity during the recovery period.

Also, from the distribution curve Full Width Half Maximum (FWHM) is calculated and shown in Table III. FWHM represents the width of the distribution characteristics in which the elements are distributed. It is noted that with the addition of alumina filler, the FWHM of Si decreases which shows the narrow distribution of the elemental intensities. The FWHM of Al distributed characteristics is higher for the 10 wt% sample due to the agglomeration of nanofiller. As a result, the observed intensity of Al peak on the sample surface varies over a wide range. The distribution characteristics of Si and Al peak for 120-minutes corona aged samples during recovery period are shown in Fig.15. Due to the breakage of the bond caused by corona ageing, the intensities of Si and Al reduce, resulting in the shift of the Si and Al distribution characteristics towards the left and the corresponding FWHM increases regardless of the filler content, as shown in Table III. Similar results were observed for all ageing periods regardless of filler content.

Further during the recovery of the corona aged samples, the distribution characteristics are shifted to the right which shows the increment in the Si and Al peak intensities. This shift clearly indicates the reorienting of the polymer chain (-CH_3) and regaining of the material surface properties. It can be seen that the distribution properties of the samples are recovered in almost 8 hours of recovery time.

H. Temporal Characteristics of LIBS emission spectra

Fig. 16 shows the temporal persistent time of the LIBS emission spectra of unaged and corona aged silicone rubber nanocomposites. When the induced plasma started to cool after the laser pulse is terminated, the excited electrons return to the ground state by making the plasma emit photons. The temporal persistence time of the LIBS emission spectra is measured by capturing the emitted light using the photodiode [29]. The addition of an alumina nanofiller increases the intensity of the emitted spectra and the cooling period as confirmed by the observed increase of the initial magnitude and mean a lifetime of the sample with an increasing filler content. The persistence time of the plasma emission spectra varies with the capacity of the species emitted during the impact of the laser pulse. This suggests that the temporal characteristics of emission spectra can be used to study the elemental variation in the samples. The temporal characteristics of the emission spectra follow an exponential decay, which is mathematically expressed as

$$V(t) = V_0 e^{-\frac{t}{\tau}} \quad (5)$$

where τ is the decay time, which was termed as emission persistence time and V_0 is the initial magnitude.

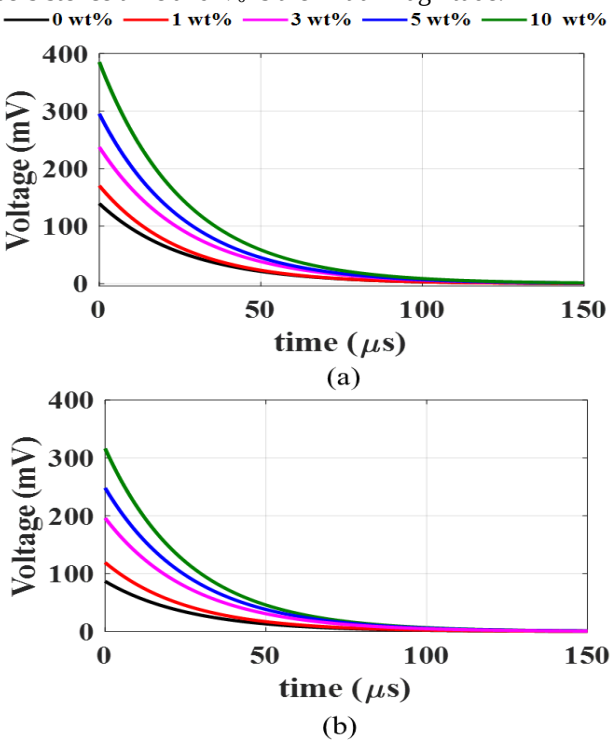

Fig. 16. LIBS emission spectra temporal persistence of silicone rubber nanocomposites (a) unaged, (b) 120 minutes corona aged.

In the case of the corona aged samples, corona ageing initiates different chain scission processes over the surface of the sample that lead to the removal of the -CH_3 functional group from the silicone rubber and surface degradation of the sample. This process eventually decreases the initial magnitude and the emission persistence time of the temporal curve for all the samples as shown in Fig. 16b. The 0 wt% sample shows a larger reduction in both persistence time and magnitude compared to other samples, proving high surface damage caused by corona

ageing. Therefore, the surface roughness and the emission spectra temporal characteristics are directly correlated. The variation in the parameters of the emission spectra temporal characteristics of unaged and 120 minutes of corona-aged samples are shown in Table IV, and a similar trend is observed for all the corona ageing periods.

During the recovery period, the silicon-oxygen bond present in the LMW components would reorient the -CH_3 functional group. This recovery in the polymer chain bonding structure increases the initial magnitude and the persistence time of the emission spectra over a period of recovery. The rate of recovery is dependent on the ease of migration of the LMW components from the bulk material to the surface. The parameters of the temporal recovery characteristics for the 0wt% and 5 wt% samples after 120 minutes of corona exposure are shown in Table V. The recovery in the persistence lifetime is faster for the 0 wt% silicone rubber sample and slower for the 5 wt% sample. This is due to the strong interaction between the nanoparticle and the polymer matrix restricting the movement of the LMW component. Further, the temporal characteristics of all nanocomposites are recovered in almost 8 hours of recovery time, as was observed from the surface roughness results presented in Section II. B.

TABLE IV
INITIAL MAGNITUDE AND PERSISTENCE TIME UNAGED AND CORONA AGED SILICONE RUBBER NANOCOMPOSITE

Sample	Initial magnitude (mV)		Persistence time (µs)	
Wt%	Unaged	120 min aged	Unaged	120 min aged
0	139.3	84.81	26.665	25.16
1	170.7	126.6	26.684	25.34
3	237.4	198.4	27.44	26.02
5	290.6	248.3	27.86	26.68
10	385.4	316.6	27.88	25.92

TABLE V
INITIAL MAGNITUDE AND PERSISTENCE TIME AGED SILICONE RUBBER NANOCOMPOSITE

Recovery time (hr)	Initial magnitude (mV)		Persistence Time (µs)	
	0 wt%	5 wt%	0 wt%	5 wt%
0	86.81	248	25.16	26.62
2	101.8	253	25.34	26.68
4	119.2	271	25.76	26.68
8	122	281.3	26.26	27.12
24	133	298.6	26.46	27.32

IV. CONCLUSIONS

The following important conclusions are obtained based on the present study,

1. The addition of nanofillers to silicone rubber suppressed the surface roughness of the specimen caused by corona ageing. 5 wt% nano alumina added silicone rubber nanocomposites is found to be the optimum nanofiller content giving a discharge resistant sample.
2. The recovery rate of surface roughness is high for pure silicone rubber but reduces with the addition of alumina nanofiller and increases with the nanofiller agglomeration. Also, the recovery rate of the surface roughness increases with the corona ageing period.
3. The hydrophobicity of all samples decreases with the corona ageing and the addition of nanofiller suppresses the hydrophobicity loss due to corona ageing.
4. Hydrophobicity of pure silicone rubber recovers fast and the addition of alumina nanofiller suppressed the hydrophobicity recovery rate. Irrespective of the corona ageing time of silicone rubber nanocomposites, the rate of recovery of hydrophobicity and surface roughness is high in the initial few hours, after corona ageing.
5. Using LIBS analysis, the normal distribution of spectral intensity of silicon and alumina was observed and the shift of the intensity distribution curve is used as a measure to assess the impact of corona discharge and recovery behavior after corona ageing.
6. The LIBS emission spectra persistence time and magnitude of the temporal characteristics were used to analyse the level of corona ageing. Also, during recovery period, the spectral persistence characteristics were found to be reach their original value.
7. The recovery characteristics of the surface roughness measured using AFM studies, hydrophobicity using static contact angle, and distribution of emission spectra and temporal behavior due to corona ageing showed a direct correlation

ACKNOWLEDGEMENT

Author (RS) wishes to thank CPRI, Bangalore, India for sponsoring the project (NPP/2016/TR/1/27042016) on nanocomposites.

REFERENCES

[1] E. A. Cherney, R. S. Gorur, and J. T. Burnham, Outdoor Insulators. Ravi s Gorur Inc, Arizona USA, 1999.

[2] S. M. Gubanski, "Modern outdoor insulation - concerns and challenges,"*IEEE Electr. Insul., Mag*, vol. 21, no. 6, pp. 5–11, Nov, 2005, doi: 10.1109/MEI.2005.1541483.

[3] S. Ilhan, D. Tuzun and A. Ozdemir, "Comparative Properties of HTV Silicone Rubber for Composite Insulators—ATH and Silica Fillers," *IEEE Trans. Dielectr. Electr. Insul*., 28, no. 2, pp. 414-422, April, 2021, doi: 10.1109/TDEI.2020.009183.

[4] D. Ghosh, D. Khastgir, "Degradation and stability of polymeric highvoltage insulators and prediction of their service life through environmental and accelerated aging processes", *ACS Omega*, Vol. 3, pp. 11317-11330, 2018, doi: 10.1021/acsomega.8b01560.

[5] K. K. Khanum, A. M. Sharma, F. Aldawsari, C. Angammana, and S. H. Jayaram, "Influence of Filler-Polymer Interface on Performance of Silicone Nanocomposites," *IEEE Trans. Ind. Appl*., vol. 56, no. 1, pp. 686–692, Jan, 2020, doi: 10.1109/TIA.2019.2943445.

[6] R. Han, Y. Li, Q. Zhu, and K. Niu, "Research on the preparation and thermal stability of silicone rubber composites: A review," *Compos. Part C Open Access*, vol. 8, pp. 100249, Aug, 2022, doi: 10.1016/j.jcomc.2022.100249.

[7] B. Venkatesulu and M. J. Thomas, "Erosion resistance of alumina-filled silicone rubber nanocomposites," *IEEE Trans. Dielectr. Electr. Insul*., vol. 17, no. 2, pp. 615–624, April, 2010, doi: 10.1109/TDEI.2010.5448119.

[8] B. Thangabalan, R. Sarathi, N. Harid, and H. Griffiths, "Analysis of space charge and charge trap characteristics of gamma irradiated silicone

rubber nanocomposites," *IET Nanodielectrics*, vol. 3, no. 2, pp. 44–52, Jun, 2020, doi: 10.1049/iet-nde.2019.0041.

[9] M. T. Nazir, B. T. Phung, and M. Hoffman, "Performance of silicone rubber composites with SiO2 micro/nano-filler under AC corona discharge," IEEE Trans. Dielectr. Electr. Insul., vol. 23, no. 5, pp. 2804–2815, Oct, 2016, doi: 10.1109/TDEI.2016.7736840.

[10] M. Akbar, R. Ullah, and S. Alam, "Aging of silicone rubber-based composite insulators under multi-stressed conditions: an overview," Mater. Res. Express, vol. 6, no. 10, Nov, 2019, doi: 10.1002/pen.25610.

[11] a M. Bi, R. Deng, T. Jiang, X. Chen, A. Pan and L. Zhu, "Study on Corona Aging Characteristics of Silicone Rubber Material Under Different Environmental Conditions,"*IEEE Transactions on Dielectrics and Electrical Insulation*, vol. 29, no. 2, pp. 534-542, April 2022, doi: 10.1109/TDEI.2022.3163792.

[12] S. Banerjee and D. Shakthi Prasad, "AC Corona Degradation of Silicone Rubber Nanocomposites at Low Air Pressure," *IEEE Trans. Dielectr. Electr. Insul.*, vol. 9878, pp. 1–1, March, 2022, doi: 10.1109/TDEI.2022.3168338.

[13] S. Li, R. Zhang, S. Wang, and Y. Fu, "Plasma treatment to improve the hydrophobicity of contaminated silicone rubber — the role of LMW siloxanes," *IEEE Trans. Dielectr. Electr. Insul.*, vol. 26, no. 2, pp. 416–422, April, 2019, doi: 10.1109/TDEI.2018.007732.

[14] M. Bi, J. Yang, X. Chen, T. Jiang, A. Pan, and Y. Dong, "The Research on Corona Aging Silicone Rubber Materials' NMR Characteristics," *IEEE Access*, vol. 8, pp. 128407–128415, July, 2020, doi: 10.1109/ACCESS.2020.3008785.

[15] Y. Zhu, "Influence of corona discharge on hydrophobicity of silicone rubber used for outdoor insulation," *Polym. Test.*, vol. 74, no. November 2018, pp. 14–20, April, 2019, doi: 10.1016/j.polymertesting.2018.12.011.

[16] Y. Gao et al., "Effects of liquids immersion and drying on the surface properties of HTV silicone rubber: characterisation by contact angle and surface physical morphology," *High Volt.*, vol. 4, no. 1, pp. 49–58, Mar, 2019, doi: 10.1049/hve.2018.5071.

[17] X. Wang et al., "Surface Hardness Analysis of Aged Composite Insulators via Laser-Induced Plasma Spectra Characterization," *IEEE Trans. Plasma Sci.*, vol. 47, no. 1, pp. 387–394, Jan, 2019, doi: 10.1109/TPS.2018.2870302.

[18] X. Wang, H. Wang, C. Chen, and Z. Jia, "Ablation Properties and Elemental Analysis of Silicone Rubber Using Laser-Induced Breakdown Spectroscopy," *IEEE Trans. Plasma Sci.*, vol. 44, no. 11, pp. 2766–2771, Nov, 2016, doi: 10.1109/TPS.2016.2586185.

[19] D. S. Prasad and B. S. Reddy, "Image saturation as a tool to understand the corona induced degradation of polymeric insulators," *IEEE Trans. Dielectr. Electr. Insul.*, vol. 27, no. 6, pp. 1837–1844, Dec. 2020, doi: 10.1109/TDEI.2020.009026.

[20] M. Z. Saleem, M. Akbar and S. Alam, "Aging Assessment of Corona-Exposed HTV-SiR/EPDM blends loaded with nanofillers," *IEEE Transactions on Plasma Science*, vol. 49, no. 12, pp. 3897-3906, Dec. 2021, doi: 10.1109/TPS.2021.3128768.

[21] Neelmani, B. Thangabalan, N. J. Vasa, B. Srinivasan, H. Suematsu, and R. Sarathi, "Investigation on Surface Condition of the Corona-Aged Silicone Rubber Nanocomposite Adopting Wavelet and LIBS Technique," *IEEE Trans. Plasma Sci.*, vol. 49, no. 8, pp. 2294–2304, Aug. 2021, doi: 10.1109/TPS.2021.3094124.

[22] Y. Yuan and T. R. Lee, "Contact Angle and Wetting Properties," Springer Berlin Heidelberg, 2013, pp. 3–34.

[23] M. T. Nazir, B. T. Phung, S. Yu, and S. Li, "Resistance against AC corona discharge of micro-ATH/nano-Al2O3 co-filled silicone rubber composites," *IEEE Trans. Dielectr. Electr. Insul.*, vol. 25, no. 2, pp. 657–667, April, 2018, doi: 10.1109/TDEI.2018.006914.

[24] J. V. Vas and M. J. Thomas, "Surface degradation of silicone rubber nanocomposites due to DC corona discharge," *IEEE Trans. Dielectr. Electr. Insul.*, vol. 21, no. 3, pp. 1175–1182, Jun, 2014, doi: 10.1109/TDEI.2014.6832263.

[25] F. Anabitarte, A. Cobo, and J. M. Lopez-Higuera, "Laser-Induced Breakdown Spectroscopy: Fundamentals, Applications, and Challenges," *ISRN Spectrosc.*, vol. 2012, pp. 1–12, Oct, 2012, doi: 10.5402/2012/285240.

[26] Z. Wang et al., "Electrochemical impedance study of water transportation in corona-aged silicone rubber: effect of applied voltage," *J. Mater. Sci.*, vol. 53, no. 18, pp. 12871–12884, June, 2018, doi: 10.1007/s10853-018-2523-x.

[27] W. Cao et al., "Study on the Law of Water Drop Movement on the Surface of Insulators under AC and DC Electric Field," in Annual Report - Conference on Electrical Insulation and Dielectric Phenomena, CEIDP, 2019, vol. no. 1, pp. 243–246, Oct ,2019, doi: 10.1109/CEIDP47102.2019.9009765.

[28] H. Belhiteche, S. Rondot, M. Moudoud, P. Dony, and O. Jbara, "Electrical insulation properties of silicone rubber under accelerated corona and thermal aging," Polym. Eng. Sci., vol. 61, no. 3, pp. 706–715, Mar. 2021, doi: 10.1002/pen.25610.

[29] H. Rajavelu, N. J. Vasa, and S. Seshadri, "Laser-Induced Breakdown Spectroscopy Combined with Temporal Plasma Analysis of C 2 Molecular Emission for Carbon Analysis in Coal," *Appl. Spectroscopy.*, vol. 75, no. 7, pp. 893–900, July, 2021, doi: 10.1177/00037028211012399.

BASKAR THANGABALAN is a Research Scholar with the High Voltage Laboratory, Department of Elec- trical Engineering, IIT Madras, Chennai, India. His research interest includes the design of nanocomposite insulating materials for outdoor applications.

NEELMANI finished his Ph.D. in High Voltage Engineering at the Department of Electrical Engineering, IIT Madras, Chennai, India. His research interests include nanoparticle generation and the design of nanocomposite insulating materials for power apparatus.

N. J. VASA is currently a Professor with the Department of Engineering Design, IIT Madras, Chennai, India. He specializes in optical and laser spectroscopy.

RAMANUJAM SARATHI (Senior Member, IEEE) received the Ph.D. degree in high voltage engineering from the Indian Institute of Science, Bangalore, India, in 1994.

He is currently a Professor and the Head of High Voltage Laboratory, Department of Electrical Engineering, IIT Madras, Chennai, India. His research interests include condition monitoring of power apparatuses and nanomaterials

NOUREDDINE HARID received the degree Ingénieur D'Etat in electrical engineering from Algiers Polytechnic, El Harrach, Algeria, in 1985, and the Ph.D. degree in electrical engineering from Cardiff University, Cardiff, U.K., in 1991. Between 1991 and 2013, he was an Assistant Professor and then an Associate Professor for different universities in different countries. Since 2013, he has been an Associate Professor with Khalifa University, Abu Dhabi, United Arab Emirates, where he conducts research in high voltage insulation, earthing systems and condition monitoring. Dr. Harid is a Member of the IET, a Fellow of the Higher Education Academy, and a Member of the BSI GEL/81 Standard Committee on Lightning Protection.

HUW GRIFFITHS received the B.Sc. degree in electrical and electronic engineering from the Polytechnic of Wales, Cardiff, U.K., and the Ph.D. degree in electrical engineering from Cardiff University, Cardiff, U.K. Between 1983 and 1990, he was an Engineer in distribution and transmission system design for SWaEB and CEGB respectively. Joining Cardiff University in 1990 as a Lecturer, and researching with the high voltage group, he became a Senior Lecturer, a Reader and a Professor. In 2015, he was a Professor with Khalifa University of Science and Technology, Abu Dhabi, UAE. He is currently honorary visiting professor in Cardiff University, UK. His research interests include grounding systems, transients and high voltage insulation. Dr. Griffiths is a Chartered Engineer, and a Member of IET. He has also been a member of several British Standards, CENELEC, IEC, CIGRE, and CIRED committees and working groups related to grounding systems.